scientific reports

Check for updates

OPEN

Entanglement and quantum correlations in the XX spin-1/2 honeycomb lattice

Sahar Satoori[1,3], Saeed Mahdavifar[1,3] & Javad Vahedi[2,3]✉

The ground state phase diagram of the dimerized spin-1/2 XX honeycomb model in presence of a transverse magnetic field (TF) is known. With the absence of the magnetic field, two quantum phases, namely, the Néel and the dimerized phases have been identified. Moreover, canted Néel and the paramagnetic (PM) phases also emerge by applying the magnetic field. In this paper, using two powerful numerical exact techniques, Lanczos exact diagonalization, and Density matrix renormalization group (DMRG) methods, we study this model by focusing on the quantum correlations, the concurrence, and the quantum discord (QD) among nearest-neighbor spins. We show that the quantum correlations can capture the position of the quantum critical points in the whole range of the ground state phase diagram consistent with previous results. Although the concurrence and the QD are short-range, informative about long-ranged critical correlations. In addition, we address a "magnetic-entanglement" behavior that starts from an entangled field around the saturation field.

The dimerization phenomenon can emerge at zero-temperature behavior of low-dimensional spin-1/2 systems. Interactions favor the spin-singlet (or triplet) between pair of spins, and therefore the ground state is a superposition of dimer states. The quantum dimer systems were initially proposed as a mapping of the lattice Bose gas to the quantum antiferromagnets[1].

In the past two decades, searching for spin-1/2 dimerized honeycomb structures has attracted much interest from an experimental point of view[2–12]. Many materials have been realized as dimerized spin-1/2 honeycomb antiferromagnets. For example, $Cu_2A_2O_7$ is known as a distorted honeycomb lattice[8]. A phase transition to an antiferromagnetic ordered state at $0.77K$ is reported for the Verdazyle radical $2-Cl-3,6-F_2-V$[9]. In addition, no long-range magnetic order is observed down to $0.6K$ in the specific heat measurements of a polycrystalline sample of the spin-1/2 distorted honeycomb lattice antiferromagnetic $Cu_2A_2O_7$[10]. In very recent work, it is shown that two antiferromagnetic interactions lead to the formation of a honeycomb lattice in some verdazyl-based complexes[12].

Theoretically, the effect of dimerization on the physics of spin-1/2 honeycomb lattices was the subject of many studies. In absence of the dimerization, it is known to realize Néel long-range order phase at zero temperature[13–17]. In the presence of dimerization, transforming the spin system onto a nonlinear sigma model, the ground state phase diagram consisting Néel and disordered spin gap phases has been proposed[18]. The mentioned quantum phase transition is confirmed by numerical quantum Monte Carlo[19] and tensor renormalization-group method[20]. By presenting the randomness on the exchange interaction in a spin-1/2 honeycomb lattice, a quantum spin liquid phase appears in the ground state phase diagram[21,22]. By doing triplon analysis and quantum Monte Carlo calculations, a spin-1/2 Heisenberg model on the honeycomb lattice with three different antiferromagnetic exchange interactions is also studied[23]. The existence of plateau states are reported in the magnetization process in this model. Also, the spin-1/2 dimerized model on a honeycomb lattice with antiferromagnetic and ferromagnetic interactions is systematically studied using the continuous-time quantum Monte Carlo method[24–26].

In recent years, powerful approaches based on the concepts borrowed from the quantum information theory[27] have been developed and intensively used to identify quantum critical points in different complex many-body systems[28]. In particular, the detailed analysis of various bipartite quantum correlations as the entanglement and the QD, has been successfully exploited to tackle many complicated problems[29–53].

Motivated by this, we study the 2D dimerized spin-1/2 XX honeycomb model in the presence of a TF. We have used the exact numerical Lanczos and DMRG techniques to probe entanglement features with dimerizatoin

[1]Department of Physics, University of Guilan, 41335-1914 Rasht, Iran. [2]Department of Physics and Earth Sciences, Jacobs University Bremen, Bremen 28759, Germany. [3]These authors contributed equally: Sahar Satoori, Saeed Mahdavifar and Javad Vahedi. ✉email: j.vahedi@jacobs-university.de

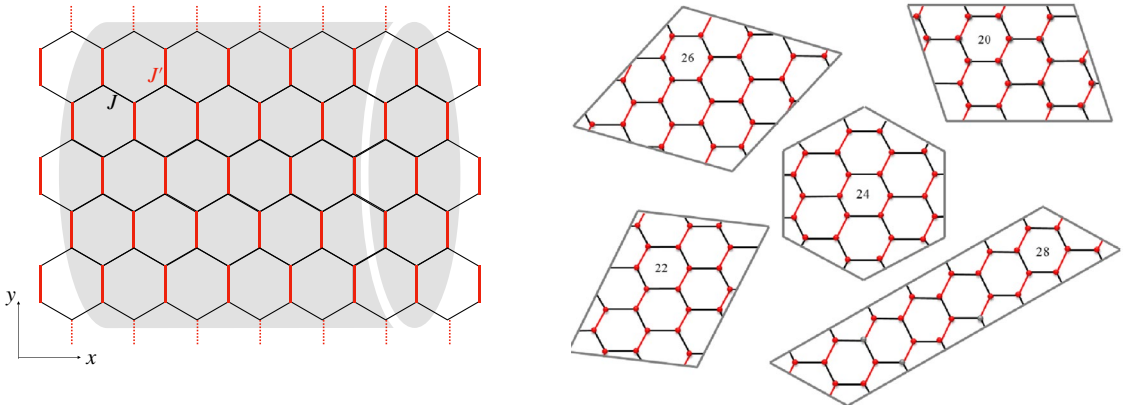

Figure 1. Schematic picture of the honeycomb lattice with different antiferromagnetic interaction coupling J and J', as shown in black and red lines, respectively. The left panel shows a cylindrical cluster considered only within the numerical DMRG method, with the periodic boundary in the y-direction. The right panel shows finite-size flak clusters considered within the numerical Lanczos method, which the twist-periodic boundary is considered.

parameter parameter. The dimerization parameter is defined as $\alpha = J/J'$ (shown on Fig. 1)). Two kinds of pairs can be considered: (1) on a bond with coupling J, (2) on a bond with coupling J'. Our numerical results show that entanglement between pairs of spins on J-bonds, signaled the quantum critical point between the Néel and the dimerized phases. By applying the TF, a magnetic entanglement is recognized that starts from a critical entangled field around the saturation field. This phenomenon was observed in one-dimensional spin-1/2 systems[54–56], and to the best of our knowledge has not been reported in a two-dimensional system. In addition, all ground-state phases have discussed from the viewpoint of quantum correlations.

The rest of the paper is organized as follows. In the next section, the model is introduced. In "Quantum correlation", a short review of quantum correlations as the entanglement and the QD are given. "Numerical results" presents numerical Lanczos and DMRG results on finite-size clusters. Finally, in "Conclusion", we summarize our conclusion.

Model

In this section, we consider the antiferromagnetic dimerized XX model on the honeycomb lattice. The Hamiltonian is defined as

$$H = J \sum_{<i,j>} (S_i^x S_j^x + S_i^y S_j^y) + J' \sum_{<i,j>'} (S_i^x S_j^x + S_i^y S_j^y) - h \sum_{i=1} S_i^z, \tag{1}$$

where S_i is the spin-$\frac{1}{2}$ operator on the i-th site of the lattice. $< i, j >$ and $< i, j >'$, with different antiferromagnetic interaction exchange couplings J and J' respectively, run over all the nearest neighbours (as schematic picture in Fig. 1). h denotes the TF. In absence of the TF, $h = 0$, a critical dimerization value α_c which separates the Néel and the dimerizad phases. At region with $\alpha < \alpha_c$, a phase transition into the paramagnetic (PM) phase anticipate occurs at the critical saturation field $h = h_s(\alpha)$. However, in the dimerized phase, two quantum phase transitions have been reported[20]. First, model undergoes a phase transition from the dimerized into the canted Néel phase at $h = h_{c_1}(\alpha)$. Second, by more increasing the TF, system goes to the PM phase at $h = h_s(\alpha)$.

The theoretical quantum study of such a physical problem requires appropriate handling of very high-rank matrices. Although the matrix of the Hamiltonian is sparse, using the standard methods it is not possible to solve the problem by direct diagonalization of a very large matrix. In the following, we apply two of the most impressive numerical tools, called the numerical Lanczos and DMRG methods for computing ground state of the Hamiltonian and then extract quantum correlations on finite size systems. The numerical Lanczos method with appropriate implementations has emerged as one of the most applicable computational procedures, mainly when the ground state is desired[57].

Although the numerical Lanczos technique allows for the exact analyses of the model's ground state, the disadvantage is, of course, its limitation to small system sizes. To study bigger system sizes, one idea is the matrix-product state (MPS) based methods, such as density matrix renormalization group (DMRG)[58,59]. The DMRG gives access to the ground state wave-function from which one can compute observable. The DMRG calculations in this paper performed using the ITensor C++ library (version 3.1)[60]. We run sweeps for the entropy to converge to at least 10^{-10}, and a large number of states, up to 1000, was kept so that the truncation error is less than 10^{-12}.

Quantum correlation

Quantum correlations have become central for the characterization and classification of many-body quantum systems. Peculiar zero-temperature quantum phases such as spin liquids[61,62], topological[63–65], and many-body localized systems[66–68] find their hallmarks in their quantum correlation features. It should be noted that the entanglement in many-body systems can be accessible in experiments such as in full-state tomography[69,70]

and ultra-cold atoms to measure Renyi entropies[71,72]. Besides, quantum phase transitions are signaled by a universal quantum correlation contribution determined solely by the universality class of the quantum phase transitions[73–78]. Hence, they can be used to detect quantum phase transitions without prior knowledge of the nature of the transition.

For a pair of spin-1/2 particles, it has been shown that the concurrence which is essentially equivalent to the entanglement of formation, can be taken as a measure of entanglement. The concurrence between two spins at sites i and j is determined by the corresponding reduced density matrix ρ_{ij},

$$\rho_{ij} = \begin{pmatrix} X_{ij}^{+} & 0 & 0 & 0 \\ 0 & Y_{ij}^{+} & Z_{ij}^{*} & 0 \\ 0 & Z_{ij} & Y_{ij}^{-} & 0 \\ 0 & 0 & 0 & X_{ij}^{-} \end{pmatrix}, \tag{2}$$

where non-zero elements of the density matrix are given by

$$\begin{aligned} X_{ij}^{+} &= \langle (1/2 + S_i^z)(1/2 + S_j^z) \rangle, \\ Y_{ij}^{+} &= \langle (1/2 + S_i^z)(1/2 - S_j^z) \rangle, \\ Y_{ij}^{-} &= \langle (1/2 - S_i^z)(1/2 + S_j^z) \rangle, \end{aligned} \tag{3}$$

$$\begin{aligned} X_{ij}^{-} &= \langle (1/2 - S_i^z)(1/2 - S_j^z) \rangle, \\ Z_{ij} &= \langle S_i^{+} S_j^{-} \rangle. \end{aligned} \tag{4}$$

The concurrence is obtained by the following expression:

$$C_{ij} = 2 \max \{0, |Z_{ij}| - \sqrt{X_{ij}^{+} X_{ij}^{-}}\}. \tag{5}$$

One should notes that, there are different quantum correlations that are not spotlighted by the entanglement measures. These quantum correlations are thoroughly included in the formulation of so-called the QD as a measure for representing all quantum correlations[79–83]. It is defined as the difference between the mutual information, $\mathscr{I}(\rho_{ij})$, and classical correlations $\mathscr{C}(\rho_{ij})$:

$$QD_{ij} = \mathscr{I}(\rho_{ij}) - \mathscr{C}(\rho_{ij}). \tag{6}$$

Mutual information does a measure on the correlation between pair spins S_i and S_j and is given by

$$\mathscr{I}(\rho_{ij}) = S(\rho_i) + S(\rho_j) + \sum_{\alpha=0}^{3} \lambda_\alpha \log(\lambda_\alpha), \tag{7}$$

where λ_α are eigenvalues of the reduced density matrix, ρ_{ij}. By definition new variables

$$\begin{aligned} c_1 &= 2Z_{ij}, \\ c_2 &= X_{ij}^{+} + X_{ij}^{-} - Y_{ij}^{+} - Y_{ij}^{-}, \\ c_3 &= X_{ij}^{+} - X_{ij}^{-}, \end{aligned} \tag{8}$$

the entropy is determined as

$$S(\rho_i) = S(\rho_j) = -\left[\left(\frac{1 + c_3}{2} \right) \log \left(\frac{1 + c_3}{2} \right) + \left(\frac{1 - c_3}{2} \right) \log \left(\frac{1 - c_3}{2} \right) \right]. \tag{9}$$

On the other hand, by definition

$$\begin{aligned} q_{k1} &= (-1)^k c_1 \left[\frac{\sin(\theta)\cos(\phi)}{1 + (-1)^k c_3 \cos(\theta)} \right], \\ q_{k2} &= \tan(\phi) q_{k1}, \\ q_{k3} &= (-1)^k \left[\frac{c_2 \cos(\theta) + (-1)^k c_3}{1 + (-1)^k c_3 \cos(\theta)} \right], \\ \theta_k &= \sqrt{q_{k1}^2 + q_{k2}^2 + q_{k3}^2} \end{aligned} \tag{10}$$

where $0 \le \theta \le \pi, 0 \le \phi \le 2\pi$ and $k = 0, 1$. The classical correlations, $\mathscr{C}(\rho_{ij})$ can be obtained by

$$\mathscr{C}(\rho_{ij}) = \max_{\{\Pi_i^B\}} \left(S(\rho_i) - \frac{S(\rho_0) + S(\rho_1)}{2} - c_3 \cos(\theta) \frac{S(\rho_0) - S(\rho_1)}{2} \right), \tag{11}$$

where

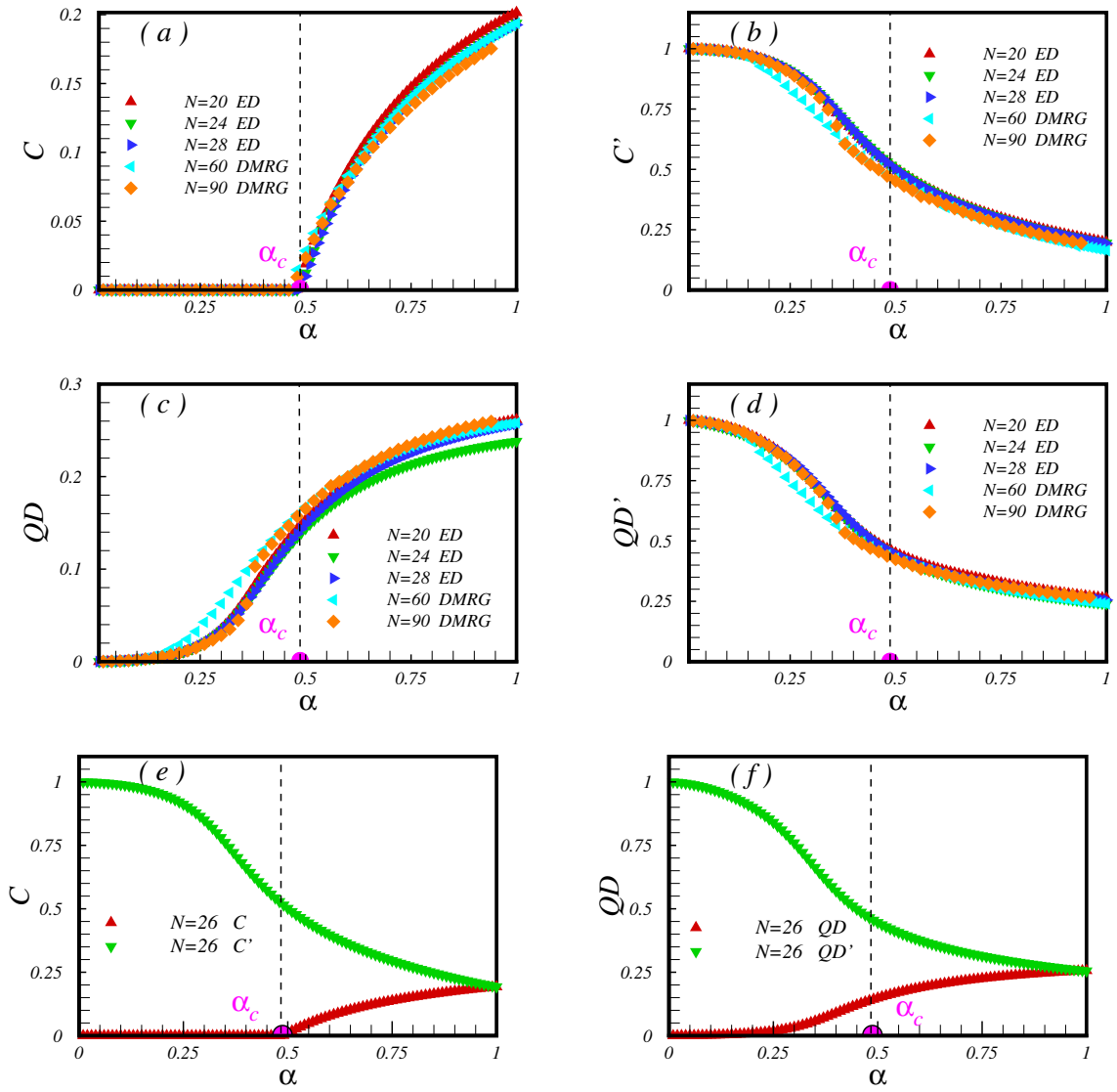

Figure 2. The concurrence and the QD between pair of spins on bonds with exchange coupling J (**a**,**c**) and J' (**b**,**d**). Lanczos results are presented for clusters with $N = 20, 24, 28$ spins and also DMRG results for $N = 60, 90$. In panels (**e**) and (**f**), concurrence and QD are plotted for a cluster with $N = 26$ spins. At $\alpha = 1$, no difference between concurrences (or values of QDs) is observed.

$$S(\rho_k) = -\left(\frac{1+\theta_k}{2}\right)\log\left(\frac{1+\theta_k}{2}\right) + \left(\frac{1-\theta_k}{2}\right)\log\left(\frac{1-\theta_k}{2}\right). \tag{12}$$

Numerical results

Here, we present the numerical results based on the Lanczos and DMRG methods. Twist periodic boundary condition (PBC) is applied for honeycomb lattice with finite flake sizes $N = 20, 24, 26, 28$ in the Lanczos technique. Moreover, we consider cylinder clusters in the DMRG method with PBC in the y-direction (as shown in Fig. 1). Having the ground state of the system, $|GS\rangle$, then quantum correlations as the concurrence and the QD are obtained.

First, we consider the model in the absence of a magnetic field. In Fig. 2, the numerical results of the concurrence and the QD between pair of spins on a bond with exchange coupling J (C) and on a bond with exchange coupling J' (C') are presented. In the case, $\alpha = 0$, the honeycomb system divides into $N/2$ individual pair spins where at zero temperature are in the singlet state (are also called dimers). Pair spins in the singlet state are maximally entangled. Consistent with this picture, numerical results in Fig. 2a,b show that, at $\alpha = 0$, only pair spins on bonds with exchange coupling J' are maximally entangled and others with exchange coupling J are unentangled. Now by turning J, what we found is interesting, the model still can be effectively treated as dimers (see panel Fig. 2a). That is almost true up to a critical point, namely α_c, which concurrence remains zero on bonds with exchange coupling J. This behavior is in agreement with expectations, based on the general statement that

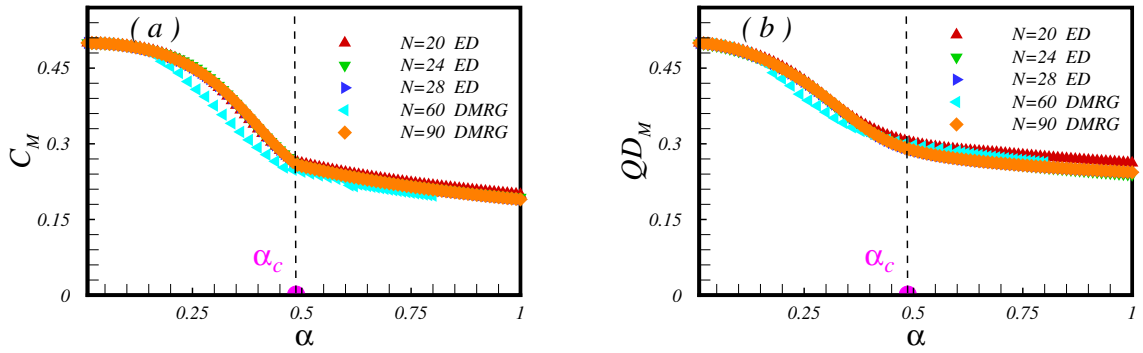

Figure 3. Mean value of the (**a**) the concurrence and (**b**) the QD versus the dimerization parameter. Signature of the quantum critical point is clearly seen in the behaviour of the concurrence.

in the gapped dimer phase, the spontaneous sublattice magnetization appears only at a finite critical value of the dimerization[20]. As soon as the dimerization parameter increases from α_c, where the model goes into the Néel phase, pair spins on bonds with exchange coupling J entangled and signature of the mentioned critical point is clearly observe in the behavior of C (see panel Fig. 2a). On the other hand, in the limit $\alpha \longrightarrow \infty$, the honeycomb system divides into individual spin-1/2 XX chains. The ground state of an individual chain system is in the Lüttinger-liquid phase and it is known that the nearest neighbours are entangled[28,29,42,43]. Consistent with this picture, our numerical results show that, only pair spins on bonds with exchange coupling J are entangled with extrapolated value $C \simeq 0.34$. Critical dimerization $\alpha_c = 0.48 \pm 0.02$ and $\alpha_c = 0.5 \pm 0.02$ are found within the Lanczos and the DMRG, respectively. The difference could pertain to the finite size effect and different clusters used on the two approaches.

In addition to the concurrence, results of the QD are plotted in Fig. 2c,d. In the case, $\alpha = 0$, QD exists only between pair of spins on dimers. Interestingly, by switching α on, QD as quantum correlations, but not necessarily involve quantum entanglement, developed between spins on bonds with J. As can be seen, QD between pair of spins on bonds with exchange coupling J' show decreasing behavior in contrast with those on bonds with exchange coupling J. Though the finite QD is an indication of a reach ground state for $0 < \alpha < \alpha_c$, it is not showing any signature as passing the quantum critical point. In the limit $\alpha \longrightarrow \infty$, where model divides into individual spin-1/2 XX chains, we found that our numerical results are in agreement with results obtained on a spin-1/2 chain model[43].

For the comparison purpose, in Fig. 2e,f concurrence and QD on different bonds are depicted. As is observed, at $\alpha = 1$ where the model becomes uniform, either concurrence or QD on different bonds cross each other. At this point, spins at two sublattices are aligned in an opposite direction to minimize the energy. It believes the model shows Néel order at zero temperature[13,16].

Within both numerical approaches, the ED and the DMRG, we probe all pairs of spins. Then we introduce a mean measurement of the concurrence and QD throughout the lattice as follows,

$$\begin{aligned} C_{\mathrm{M}} &= \frac{1}{N'} \sum_{<i,j>} C_{ij}, \\ QD_{\mathrm{M}} &= \frac{1}{N'} \sum_{<i,j>} QD_{ij}, \end{aligned} \tag{13}$$

where $N' = \frac{3}{2}N$ is the number of pair spins in each cluster of the model. Results illustrate in Fig. 3. As can be seen, C_{M} first decreases by increasing the dimerization parameter up to the quantum critical point $\alpha = \alpha_c$. As already seen, up to the critical point α_c, all entanglement contributions to C_{M} come from bonds with exchange coupling J' (bounds depicted with red color in Fig. 1). For dimerization parameter bigger than α_c spins between bonds with exchange coupling J begin to entangle, and C_{M} shows almost a different decreasing slope in the region $\alpha > \alpha_c$. Thus the quantum critical point may be detected by focusing on the mean value of entanglement between pair of spins. However, the mean value of the QD between the nearest-neighbour pair of spins do not show the quantum critical point, as shown in Fig. 3b. Indeed, for the present model, by focusing only on the QD_{M}, one could not detect the quantum critical point.

Now lets us consider the transverse magnetic field, and probe the entanglement and QD evolution throughout the model. To this end, we fix the parameter α such as the model exists (i) at the Néel phase with $\alpha > \alpha_c$, (ii) at dimerized phase with $\alpha < \alpha_c$.

Results for the case (i) with $\alpha = 0.7$ are plotted in Fig. 4. At $h = 0$, as identified before, concurrence is shared between all nearest-neighbor pair spins. By tuning the magnetic field, C shows almost increasing behaviour until the quantum critical region close to the critical point h_c where separates the Neel and PM phases (see Fig. 4a). As soon as the system enters to the quantum critical region, C decreases monotonically till disappearing at saturation filed h_s. That is expected at $h_s(\alpha) \simeq 1.14$, as all of the spins are aligned in the direction of the field. One should notes that the jumping at this point resulted of degeneracy of saturation critical point. On the other hand, as soon as the TF turns on, C' decreases and will be disappeared at the saturation TF, h_s (see Fig. 4b). No signature of the quantum critical region is seen in the behaviour of C'. It should be noted that the same behaviour as the C

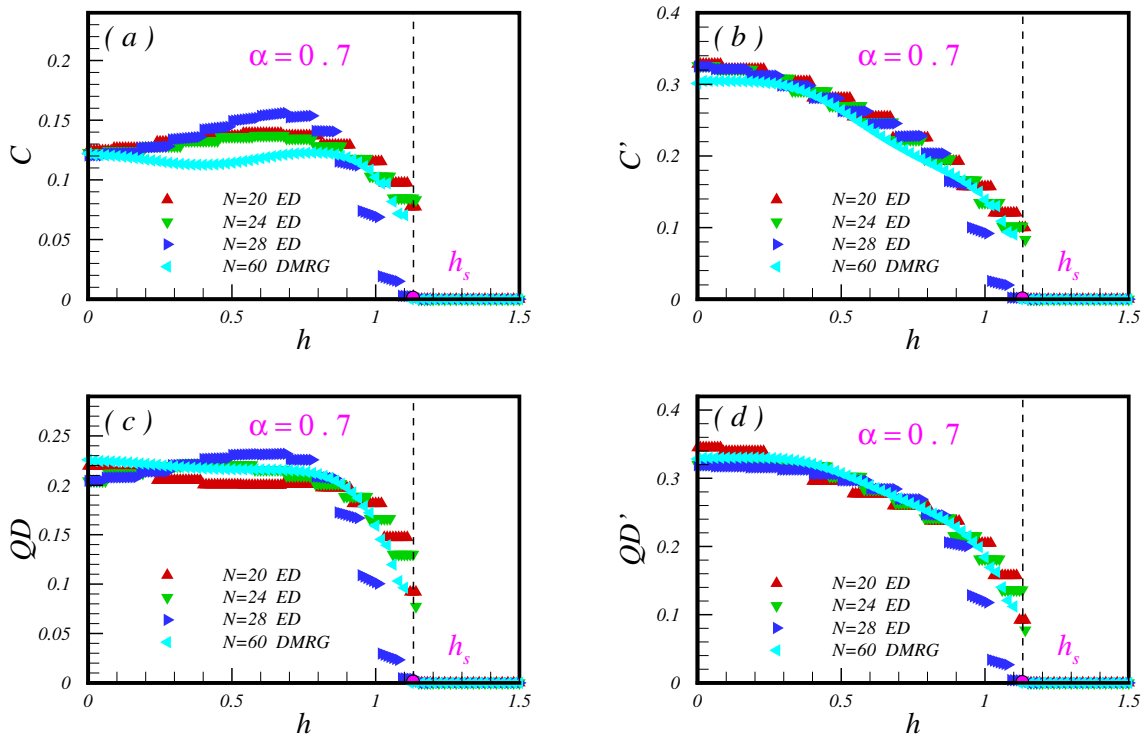

Figure 4. The concurrence and the QD between pair of spins on bonds with exchange coupling J (**a**,**c**) and J' (**b**,**d**) versus the TF. Lanczos results are presented for $\alpha = 0.7$ and clusters with $N = 20, 24, 28$ spins. DMRG results presents for $N = 60$.

and C' is observe for the QD between pair of spins on bonds with exchange coupling J (Fig. 4c) and J' (Fig. 4d). Observed oscillations of the quantum correlations result from the level crossing between the ground and the excited states of the model.

We have done the same numerical experiment when the system exists deep in the dimerized phase with $\alpha = 0.2$ and results are presented in Fig. 5. Within this parameter, the model can be effectively assumed as an ensemble of singlet pairs that are weakly interacting. It is known that by applying a TF, system remains in the gaped dimerized phase up to the first critical field $h_{c_1}(\alpha)$. With more increasing the field, the system goes to a canted Néel phase, and finally, at a saturation field $h_s(\alpha)$ becomes polarized.

Interesting behaviour is seen in the results of the concurrence between pair of spins on bonds with exchange coupling J (Fig. 5a). Despite these pair of spins are not entangled in the absence of the TF, they still remain unentangled in the canted Néel phase, which shows that low excited states of the pure dimerized model in the region $\alpha < \alpha_c$ are not entangled by considering C. More fascinating, we find the field-induced entanglement region, which we call "magnetic entanglement", by increasing the field. The magnetic field develops entanglement between pair of spins on bonds with exchange coupling J at $h = h_E(\alpha)$ and then gets profound in the region $h_E(\alpha) < h < h_s$. The emergence of the magnetic field can be understood as following: the z-component of the total spin commutes with the Hamiltonian and the ground state exists in the subspace $S_t^z = 0$ for $h = 0$ and excited states are located in subspaces with higher $S_t^z = 1, 2, \ldots, N/2$. When the TF applies, the energy of the lowest state in the subspace with $S_t^z = 1$ decreases and becomes the ground state of the system at the first critical TF, h_{c_1}. With more increasing field, the energy of excited states of the pure dimerized system decreases more and becomes the ground state of the system. Therefore, what we are capturing from our numerical experiment in presence of the TF, in principle reflects the information of the excited states of the pure dimerized model.

As can be seen from Fig. 5b,d, in absence of TF, pair of spins on bonds with exchange coupling J' are quantum correlated. These bonds remain entangled or quantum correlated with a constant value up to the first critical $h_{c_1} \simeq 0.27$. By increasing the field, C' and QD' develop a series of plateaus with a decreasing trend and vanish at the saturated field $h_s \simeq 0.67$.

Finally as is seen in Fig. 5c, QD between pair of spins on bonds with exchange coupling J, shows an almost zero-plateau up to first critical TF and exactly a zero-plateau in the region $h > h_s$. It is observed that as soon as the system enters into the canted Néel phase, QD increases up to the vicinity of the saturation field h_s. Exactly at the saturation TF, QD will be zero and no quantum correlations is observed in the PM region.

Conclusion

We considered a dimerized spin-1/2 XX honeycomb model in the presence of a transverse magnetic field. At zero temperature the ground state phase diagram is known. In the absence of the field, there is a critical dimerization point α_c, which separates the commensurate Néel and incommensurate dimer phases. In presence of the field, system becomes polarized at a saturation field, $h = h_s(\alpha)$. By placing the model at dimerized phase and changing

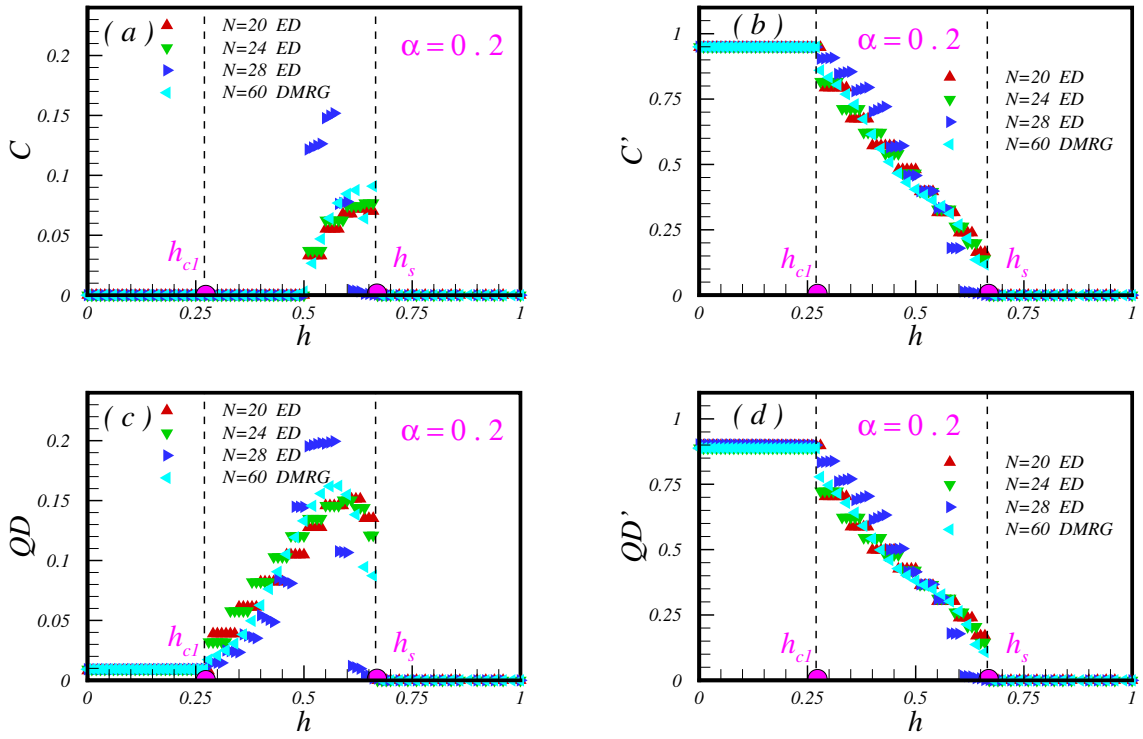

Figure 5. The concurrence and the QD between pair of spins on bonds with exchange coupling J (**a**,**c**) and J' (**b**,**d**) versus the TF. Lanczos results are presented for $\alpha = 0.2$ and clusters with $N = 20, 24, 28$ spins and also DMRG results for $N = 60$.

the field, model undergoes a quantum phase transition from the dimer into the canted Néel phase at $h_{c_1}(\alpha)$. With a more increasing field, spins finally get aligned with the field at the saturation point h_s.

Equipped with the knowledge above, we tried to understand the entanglement feature of the model. To this end, we borrowed concurrence and quantum discord (QD) observable from the quantum information context. We focused on the quantum correlations among the nearest-neighbour pair of spins on finite clusters using the complimentary numerical Lanczos and DMRG techniques. Critical dimerization point, α_c, is obtained from the concurrence. In presence of the field, we observed the "magnetic entanglement" region between $h_E(\alpha) < h < h_s(\alpha)$, which an entanglement creates between paired of unentangled spins when we had $h = 0$. Exploiting quantum entanglement features to study exotic magnetic phases at zero temperature has privileges compared to the Landau theory, as the definition of a proper order parameter is not easy. This work could potentially be extended to check the resonating valence bonds (RVB) state or quantum spin liquid (QSL) phase in the honeycomb lattice[21,22].

Data availability

The data-sets used and analysed during the current study available from the corresponding author on reasonable request.

Received: 28 April 2022; Accepted: 6 September 2022
Published online: 26 October 2022

References

1. Matsubara, T. & Matsuda, H. A lattice model of liquid helium, i. *Progress Theoret. Phys.* **16**, 569–582. https://doi.org/10.1143/ptp.16.569 (1956).
2. Kataev, V. *et al.* Structural and magnetic properties of the new low-dimensional spin magne. *J. Magn. Magn. Mater.* **290–291**, 310–313. https://doi.org/10.1016/j.jmmm.2004.11.204 (2005).
3. Spremo, I. *et al.* Magnetic properties of a metal-organic antiferromagnet on a distorted honeycomb lattice. *Phys. Rev. B* **72**, 174429. https://doi.org/10.1103/PhysRevB.72.174429 (2005).
4. Miura, Y., Hirai, R., Kobayashi, Y. & Sato, M. Spin-gap behavior of na3cu2sbo6 with distorted honeycomb structure. *J. Phys. Soc. Jpn.* **75**, 084707. https://doi.org/10.1143/jpsj.75.084707 (2006).
5. Janson, O. *et al.* Long-range superexchange in $cu_2A_2o_7$ (a = p, as, v) as a key element of the microscopic magnetic model. *Phys. Rev. B* **83**, 094435. https://doi.org/10.1103/PhysRevB.83.094435 (2011).
6. Lebernegg, S., Tsirlin, A. A., Janson, O. & Rosner, H. Spin gap in malachite $cu_2(oh)_2co_3$ and its evolution under pressure. *Phys. Rev. B* **88**, 224406. https://doi.org/10.1103/PhysRevB.88.224406 (2013).
7. Gitgeatpong, G. *et al.* Magnetic structure and dzyaloshinskii-moriya interaction in the $s = \frac{1}{2}$ helical-honeycomb antiferromagnet $\alpha-cu_2v_2o_7$. *Phys. Rev. B* **92**, 024423. https://doi.org/10.1103/PhysRevB.92.024423 (2015).
8. Sugawara, K. *et al.* Investigation of honeycomb lattice consisting of cu2(pymca)3 moieties using synchrotron radiation x-ray structure analysis. *J. Phys. Soc. Jpn.* **86**, 123302. https://doi.org/10.7566/jpsj.86.123302 (2017).

9. Okabe, T. *et al.* Magnetic properties of the $s = \frac{1}{2}$ honeycomb lattice antiferromagnet 2−Cl−3, 6−f_2−V. *Phys. Rev. B* **95**, 075120. https://doi.org/10.1103/PhysRevB.95.075120 (2017).
10. Okutani, A. *et al.* High-field magnetism of the honeycomb-lattice antiferromagnet cu2(pymca)3(ClO4). *J. Phys. Soc. Jpn.* **88**, 013703. https://doi.org/10.7566/jpsj.88.013703 (2019).
11. Miyamoto, S. *et al.* Magnetic properties of honeycomb-based spin models in verdazyl-based salts. *Phys. Rev. Mater.* **3**, 064410. https://doi.org/10.1103/PhysRevMaterials.3.064410 (2019).
12. Kono, Y. *et al.* Magnetic properties of a spin-$\frac{1}{2}$ honeycomb lattice antiferromagnet. *Phys. Rev. B* **101**, 014437. https://doi.org/10.1103/PhysRevB.101.014437 (2020).
13. Reger, J. D., Riera, J. A. & Young, A. P. Monte carlo simulations of the spin-1/2heisenberg antiferromagnet in two dimensions. *J. Phys.: Condens. Matter* **1**, 1855–1865. https://doi.org/10.1088/0953-8984/1/10/007 (1989).
14. Weihong, Z., Oitmaa, J. & Hamer, C. J. Second-order spin-wave results for the quantum xxz and xy models with anisotropy. *Phys. Rev. B* **44**, 11869–11881. https://doi.org/10.1103/PhysRevB.44.11869 (1991).
15. Fouet, J., Sindzingre, P. & Lhuillier, C. An investigation of the quantum $J_1-J_2-J_3$ model on the honeycomb lattice. *Eur. Phys. J. B* **20**, 241–254. https://doi.org/10.1007/s100510170273 (2001).
16. Jiang, H. C., Weng, Z. Y. & Xiang, T. Accurate determination of tensor network state of quantum lattice models in two dimensions. *Phys. Rev. Lett.* **101**, 090603. https://doi.org/10.1103/PhysRevLett.101.090603 (2008).
17. Xie, Z. Y., Jiang, H. C., Chen, Q. N., Weng, Z. Y. & Xiang, T. Second renormalization of tensor-network states. *Phys. Rev. Lett.* **103**, 160601. https://doi.org/10.1103/PhysRevLett.103.160601 (2009).
18. Takano, K. Spin-gap phase of a quantum spin system on a honeycomb lattice. *Phys. Rev. B* **74**, 140402. https://doi.org/10.1103/PhysRevB.74.140402 (2006).
19. Jiang, F.-J. & Gerber, U. Subtlety of determining the critical exponent ν of the spin-1/2 heisenberg model with a spatially staggered anisotropy on the honeycomb lattice. *J. Stat. Mech: Theory Exp.* **2009**, P09016. https://doi.org/10.1088/1742-5468/2009/09/p09016 (2009).
20. Li, W., Gong, S.-S., Zhao, Y. & Su, G. Quantum phase transition, $o(3)$ universality class, and phase diagram of the spin-$\frac{1}{2}$ heisenberg antiferromagnet on a distorted honeycomb lattice: A tensor renormalization-group study. *Phys. Rev. B* **81**, 184427. https://doi.org/10.1103/PhysRevB.81.184427 (2010).
21. Yamaguchi, H. *et al.* Randomness-induced quantum spin liquid on honeycomb lattice. *Sci. Rep.* **7**. https://doi.org/10.1038/s41598-017-16431-0 (2017).
22. Uematsu, K. & Kawamura, H. Randomness-induced quantum spin liquid behavior in the $s = \frac{1}{2}$ random J_1-J_2 heisenberg antiferromagnet on the square lattice. *Phys. Rev. B* **98**, 134427. https://doi.org/10.1103/PhysRevB.98.134427 (2018).
23. Adhikary, M., Ralko, A. & Kumar, B. Quantum paramagnetism and magnetization plateaus in a kagome-honeycomb heisenberg antiferromagnet. *Phys. Rev. B* **104**, 094416. https://doi.org/10.1103/PhysRevB.104.094416 (2021).
24. Huang, Y.-Z. *et al.* Quantum phase transition, universality, and scaling behaviors in the spin-1/2 heisenberg model with ferromagnetic and antiferromagnetic competing interactions on a honeycomb lattice. *Phys. Rev. E* **93**, 062110. https://doi.org/10.1103/PhysRevE.93.062110 (2016).
25. Huang, Y.-Z. & Su, G. Quantum monte carlo study of the spin-1/2 honeycomb heisenberg model with mixed antiferromagnetic and ferromagnetic interactions in external magnetic fields. *Phys. Rev. E* **95**, 052147. https://doi.org/10.1103/PhysRevE.95.052147 (2017).
26. Uwabo, Y. & Mochizuki, M. Proposed negative thermal expansion in honeycomb-lattice antiferromagnets. *J. Phys. Soc. Jpn.* **90**, 104712. https://doi.org/10.7566/jpsj.90.104712 (2021).
27. Zeng, B., Chen, X., Zhou, D.-L. & Wen, X.-G. Quantum error-correcting codes. In *Quantum Information Meets Quantum Matter*, 63–82, https://doi.org/10.1007/978-1-4939-9084-9_3 (Springer New York, 2019).
28. Amico, L., Fazio, R., Osterloh, A. & Vedral, V. Entanglement in many-body systems. *Rev. Mod. Phys.* **80**, 517–576. https://doi.org/10.1103/revmodphys.80.517 (2008).
29. Osborne, T. J. & Nielsen, M. A. Entanglement in a simple quantum phase transition. *Phys. Rev. A***66**. https://doi.org/10.1103/physreva.66.032110 (2002).
30. Osterloh, A., Amico, L., Falci, G. & Fazio, R. Scaling of entanglement close to a quantum phase transition. *Nature* **416**, 608–610. https://doi.org/10.1038/416608a (2002).
31. Vidal, G., Latorre, J. I., Rico, E. & Kitaev, A. Entanglement in quantum critical phenomena. *Phys. Rev. Lett.* **90**, 227902. https://doi.org/10.1103/PhysRevLett.90.227902 (2003).
32. Wu, L.-A., Sarandy, M. S. & Lidar, D. A. Quantum phase transitions and bipartite entanglement. *Phys. Rev. Lett.* **93**, 250404. https://doi.org/10.1103/PhysRevLett.93.250404 (2004).
33. Legeza, O. & Sólyom, J. Two-site entropy and quantum phase transitions in low-dimensional models. *Phys. Rev. Lett.* **96**, 116401. https://doi.org/10.1103/PhysRevLett.96.116401 (2006).
34. Legeza, O., Sólyom, J., Tincani, L. & Noack, R. M. Entropic analysis of quantum phase transitions from uniform to spatially inhomogeneous phases. *Phys. Rev. Lett.* **99**, 087203. https://doi.org/10.1103/PhysRevLett.99.087203 (2007).
35. Wei, T.-C. Exchange symmetry and global entanglement and full separability. *Phys. Rev. A* **81**, 054102. https://doi.org/10.1103/PhysRevA.81.054102 (2010).
36. Liu, B.-Q., Shao, B., Li, J.-G., Zou, J. & Wu, L.-A. Quantum and classical correlations in the one-dimensional XY model with dzyaloshinskii-moriya interaction. *Phys. Rev. A* **83**, 052112. https://doi.org/10.1103/PhysRevA.83.052112 (2011).
37. Ma, F.-W., Liu, S.-X. & Kong, X.-M. Entanglement and quantum phase transition in the one-dimensional anisotropic *XY* model. *Phys. Rev. A* **83**, 062309. https://doi.org/10.1103/PhysRevA.83.062309 (2011).
38. You, W. L. Quantum correlation in one-dimensional extended quantum compass model. *Eur. Phys. J. B* **85**. https://doi.org/10.1140/epjb/e2012-21046-y (2012).
39. Sarandy, M. S., Oliveria, T. R. D. & Amico, L. Quantum discord in the ground state of spin chain. *Int. J. Mod. Phys. B* **27**, 1345030. https://doi.org/10.1142/s0217979213450306 (2012).
40. Hofmann, M., Osterloh, A. & Gühne, O. Scaling of genuine multiparticle entanglement close to a quantum phase transition. *Phys. Rev. B* **89**, 134101. https://doi.org/10.1103/PhysRevB.89.134101 (2014).
41. ke Song, X., Wu, T., Xu, S., He, J. & Ye, L. Renormalization of quantum discord and bell nonlocality in the XXZ model with dzyaloshinskii-moriya interaction. *Ann. Phys.* **349**, 220–231. https://doi.org/10.1016/j.aop.2014.06.006 (2014).
42. Fumani, F. K., Nemati, S., Mahdavifar, S. & Darooneh, A. H. Magnetic entanglement in spin-1/2 XY chains. *Phys. A* **445**, 256–263. https://doi.org/10.1016/j.physa.2015.11.004 (2016).
43. Mofidnakhaei, F., Fumani, F. K., Mahdavifar, S. & Vahedi, J. Quantum correlations in anisotropic XY-spin chains in a transverse magnetic field. *Phase Trans.* **91**, 1256–1267. https://doi.org/10.1080/01411594.2018.1527916 (2018).
44. Soltani, M., Fumani, F. K. & Mahdavifar, S. Ising in a transverse field with added transverse dzyaloshinskii-moriya interaction. *J. Magn. Magn. Mater.* **476**, 580–588. https://doi.org/10.1016/j.jmmm.2018.12.019 (2019).
45. Nemati, S., Fumani, F. K. & Mahdavifar, S. Identification of unentangled–entangled border in the luttinger liquid phase. *Curr. Comput.-Aided Drug Des.* **9**, 105. https://doi.org/10.3390/cryst9020105 (2019).
46. Soltani, M. R., Mahdavifar, S., Akbari, A. & Masoudi, A. A. Metamagnetic phase transition in the 1d ising plus dzyaloshinskii–moriya model. *J. Supercond. Novel Magn.* **23**, 1369–1375. https://doi.org/10.1007/s10948-010-0785-x (2010).

47. Soltani, M., Vahedi, J. & Mahdavifar, S. Quantum correlations in the 1d spin-1/2 ising model with added dzyaloshinskii–moriya interaction. *Phys. A* **416**, 321–330. https://doi.org/10.1016/j.physa.2014.08.017 (2014).
48. Cheraghi, H. & Mahdavifar, S. Ineffectiveness of the dzyaloshinskii-moriya interaction in the dynamical quantum phase transition in the ITF model. *J. Phys.: Condens. Matter* **30**, 42LT01. https://doi.org/10.1088/1361-648x/aae1c5 (2018).
49. Li, B., Cho, S. Y., Wang, H.-L. & Hu, B.-Q. Ground state fidelity in bond-alternative ising chains with dzyaloshinskii–moriya interactions. *J. Phys. A: Math. Theor.* **44**, 392002. https://doi.org/10.1088/1751-8113/44/39/392002 (2011).
50. Amiri, N. & Langari, A. Quantum critical phase diagram of bond alternating ising model with dzyaloshinskii-moriya interaction: Signature of ground state fidelity. *Phys. Status Solidi (b)* **250**, 537–541. https://doi.org/10.1002/pssb.201200733 (2013).
51. Fumani, F. K., Beradze, B., Nemati, S., Mahdavifar, S. & Japaridze, G. Quantum correlations in the spin-1/2 heisenberg XXZ chain with modulated dzyaloshinskii-moriya interaction. *J. Magn. Magn. Mater.* **518**, 167411. https://doi.org/10.1016/j.jmmm.2020.167411 (2021).
52. Fumani, F. K., Motamedifar, M. & Mahdavifar, S. Quantum phases of the 1d anisotropic spin-1/2 frustrated ferromagnetic model: view point of quantum correlations. *Phys. Scr.* **95**, 055806. https://doi.org/10.1088/1402-4896/ab73d7 (2020).
53. Fumani, F. K., Nemati, S. & Mahdavifar, S. Quantum critical lines in the ground state phase diagram of spin-1/2 frustrated transverse-field ising chains. *Ann. Phys.* **533**, 2000384. https://doi.org/10.1002/andp.202000384 (2020).
54. Fumani, F. K., Nemati, S., Mahdavifar, S. & Darooneh, A. H. Magnetic entanglement in spin-1/2 XY chains. *Phys. A* **445**, 256–263. https://doi.org/10.1016/j.physa.2015.11.004 (2016).
55. Mahdavifar, S., Mahdavifar, S. & Jafari, R. Magnetic quantum correlations in the one-dimensional transverse-field *xxz* model. *Phys. Rev. A* **96**, 052303. https://doi.org/10.1103/PhysRevA.96.052303 (2017).
56. Nemati, S., Khastehdel Fumani, F. & Mahdavifar, S. Identification of unentangled?entangled border in the luttinger liquid phase. *Crystals***9**, https://doi.org/10.3390/cryst9020105 (2019).
57. Giuseppe Grosso, G. P. *Solid State Phys.* (Academic Press, 2013).
58. White, S. R. Density matrix formulation for quantum renormalization groups. *Phys. Rev. Lett.* **69**, 2863–2866. https://doi.org/10.1103/PhysRevLett.69.2863 (1992).
59. Schollwöck, U. The density-matrix renormalization group. *Rev. Mod. Phys.* **77**, 259–315. https://doi.org/10.1103/RevModPhys.77.259 (2005).
60. Fishman, M., White, S. R. & Stoudenmire, E. M. The ITensor software library for tensor network calculations (2020).
61. Balents, L. Spin liquids in frustrated magnets. *Nature* **464**, 199–208. https://doi.org/10.1038/nature08917 (2010).
62. Savary, L. & Balents, L. Quantum spin liquids: A review. *Rep. Prog. Phys.* **80**, 016502. https://doi.org/10.1088/0034-4885/80/1/016502 (2016).
63. Pollmann, F., Turner, A. M., Berg, E. & Oshikawa, M. Entanglement spectrum of a topological phase in one dimension. *Phys. Rev. B* **81**, 064439. https://doi.org/10.1103/PhysRevB.81.064439 (2010).
64. Jiang, H.-C., Wang, Z. & Balents, L. Identifying topological order by entanglement entropy. *Nat. Phys.* **8**, 902–905. https://doi.org/10.1038/nphys2465 (2012).
65. Haug, T., Amico, L., Kwek, L.-C., Munro, W. J. & Bastidas, V. M. Topological pumping of quantum correlations. *Phys. Rev. Res.* **2**, 013135. https://doi.org/10.1103/PhysRevResearch.2.013135 (2020).
66. Bardarson, J. H., Pollmann, F. & Moore, J. E. Unbounded growth of entanglement in models of many-body localization. *Phys. Rev. Lett.* **109**, 017202. https://doi.org/10.1103/PhysRevLett.109.017202 (2012).
67. Singh, R., Bardarson, J. H. & Pollmann, F. Signatures of the many-body localization transition in the dynamics of entanglement and bipartite fluctuations. *New J. Phys.* **18**, 023046. https://doi.org/10.1088/1367-2630/18/2/023046 (2016).
68. De Tomasi, G., Bera, S., Bardarson, J. H. & Pollmann, F. Quantum mutual information as a probe for many-body localization. *Phys. Rev. Lett.* **118**, 016804. https://doi.org/10.1103/PhysRevLett.118.016804 (2017).
69. Jurcevic, P. *et al.* Quasiparticle engineering and entanglement propagation in a quantum many-body system. *Nature* **511**, 202–205. https://doi.org/10.1038/nature13461 (2014).
70. Friis, N. *et al.* Observation of entangled states of a fully controlled 20-qubit system. *Phys. Rev. X* **8**, 021012. https://doi.org/10.1103/PhysRevX.8.021012 (2018).
71. Daley, A. J., Pichler, H., Schachenmayer, J. & Zoller, P. Measuring entanglement growth in quench dynamics of bosons in an optical lattice. *Phys. Rev. Lett.* **109**, 020505. https://doi.org/10.1103/PhysRevLett.109.020505 (2012).
72. Islam, R. *et al.* Measuring entanglement entropy in a quantum many-body system. *Nature* **528**, 77–83. https://doi.org/10.1038/nature15750 (2015).
73. Osterloh, A., Amico, L., Falci, G. & Fazio, R. Scaling of entanglement close to a quantum phase transition. *Nature* **416**, 608–610. https://doi.org/10.1038/416608a (2002).
74. Shan, C.-J., Cheng, W.-W., Liu, J.-B., Cheng, Y.-S. & Liu, T.-K. Scaling of geometric quantum discord close to a topological phase transition. *Sci. Rep.* **4**. https://doi.org/10.1038/srep04473 (2014).
75. Huang, Y. Scaling of quantum discord in spin models. *Phys. Rev. B* **89**, 054410. https://doi.org/10.1103/PhysRevB.89.054410 (2014).
76. Hauke, P., Heyl, M., Tagliacozzo, L. & Zoller, P. Measuring multipartite entanglement through dynamic susceptibilities. *Nat. Phys.* **12**, 778–782. https://doi.org/10.1038/nphys3700 (2016).
77. Radgohar, R. & Montakhab, A. Global entanglement and quantum phase transitions in the transverse xy heisenberg chain. *Phys. Rev. B* **97**, 024434. https://doi.org/10.1103/PhysRevB.97.024434 (2018).
78. Mishra, U. & Bayat, A. Driving enhanced quantum sensing in partially accessible many-body systems. *Phys. Rev. Lett.* **127**, 080504. https://doi.org/10.1103/PhysRevLett.127.080504 (2021).
79. Zurek, W. Einselection and decoherence from an information theory perspective. *Ann. Phys.* **9**, 855–864. https://doi.org/10.1002/1521-3889(200011)9:11/12<855::aid-andp855>3.0.co;2-k (2000).
80. Ollivier, H. & Zurek, W. H. Quantum discord: A measure of the quantumness of correlations. *Phys. Rev. Lett.* **88**, 017901. https://doi.org/10.1103/PhysRevLett.88.017901 (2001).
81. Henderson, L. & Vedral, V. Classical, quantum and total correlations. *J. Phys. A: Math. Gen.* **34**, 6899–6905. https://doi.org/10.1088/0305-4470/34/35/315 (2001).
82. Zurek, W. H. Decoherence, einselection, and the quantum origins of the classical. *Rev. Mod. Phys.* **75**, 715–775. https://doi.org/10.1103/revmodphys.75.715 (2003).
83. Bera, A. *et al.* Quantum discord and its allies: A review of recent progress. *Rep. Prog. Phys.* **81**, 024001. https://doi.org/10.1088/1361-6633/aa872f (2017).

Author contributions

S.S. and S.M. conducted the Lanczos numerical calculations, J.V. prepared the DMRG data. All authors reviewed the manuscript.

Funding

Open Access funding enabled and organized by Projekt DEAL.

Competing interests
The authors declare no competing interests.

Additional information
Correspondence and requests for materials should be addressed to J.V.

Reprints and permissions information is available at www.nature.com/reprints.

Publisher's note Springer Nature remains neutral with regard to jurisdictional claims in published maps and institutional affiliations.